PAPER

Check for updates

Activation of ZrO$_2$–WO$_3$ solid acid catalysts in a Friedel–Crafts reaction through post-hydrothermal treatment†

Sha Li, [ID] * Ruopeng Yu, Bonan Xu, Zhikun Wang, Chunzheng Wu [ID] *
and Jianzhong Guo*

ZrO$_2$–WO$_3$ mixed oxide plays an essential role in the chemical and petroleum industries. So far, very little work has paid attention to the activation of the low activity of ZrO$_2$–WO$_3$ catalysts. In this work, poorly reactive ZrO$_2$–WO$_3$ was prepared as a model catalyst by a sol–gel method and it was accompanied by post-hydrothermal treatment with various solutions. The catalytic results in the Friedel–Crafts reaction of anisole and benzyl alcohol showed that the post-hydrothermal treatment with ethylenediamine or ammonium hydroxide solutions dramatically improved the activity of ZrO$_2$–WO$_3$, while the hydrothermal treatments with water or ammonia chloride solution resulted in poorer activity and selectivity. The former treatments were found to induce a huge transformation of the ZrO$_2$ crystal from monoclinic to tetragonal as well as a significant increase in acidic WO$_x$ clusters that anchored onto ZrO$_2$. The generation of the WO$_x$ clusters was responsible for the activation of ZrO$_2$–WO$_3$.

Introduction

Solid acid catalysts are of great importance in the chemical and petroleum industries not only because of their advantages in the separation of products, but also due to their good stability against corrosion. Among the abundant solid acid catalysts, WO$_3$–ZrO$_2$, that was first reported by Hino and Arata,[1–3] has attracted much attention in last decades due to its high activity in various acid reactions and high mechanical and thermal stability that allows it to work in harsh conditions (like oxidative/reductive and H$_2$O environments). Basically, the acidity and activity of WO$_3$–ZrO$_2$ originate from sub-nanometer WO$_x$ clusters, which could be largely impacted by the phase of the ZrO$_2$,[4,5] the content of tungsten,[6–11] calcination temperature[12,13] or more generally the preparation methods applied.[14–16]

The hydrothermal method is one of the most popular ways for the synthesis of ZrO$_2$–WO$_3$. It usually results in a stronger zirconium–tungsten interaction compared to precipitation–calcination and sol–gel methods.[17] This strong interaction is proposed to cause a better dispersion of WO$_3$ and generates more acid sites.[18,19] On the other hand, hydrothermal conditions affect the size, morphology, composition, and structure of

Key Laboratory of Chemical Utilization of Forestry Biomass in Zhejiang Province, College of Chemistry and Materials Engineering, Zhejiang A & F University, Hangzhou 311300, China. E-mail: shali@zafu.edu.cn; wucz@zafu.edu.cn; guojianzhong@zafu.edu.cn

† Electronic supplementary information (ESI) available: XPS, repeated experiments, N$_2$ adsorption–desorption curve, XRD and Tables S1 and S2. See https://doi.org/10.1039/d2ra00519k

the products. For instance, hydrothermal treatment at improved temperatures was reported by Zhou *et al.* to affect the structural deformation of ZrO$_2$ (*i.e.*, causing more tetragonal ZrO$_2$), which resulted in stronger surface acidity.[20]

Noteworthy, most of the reported hydrothermal method was applied to the synthesis process of catalysts and very little attention has been paid to the post-activation of a poor catalyst. In the present work, we found for the first time that a suitable post-hydrothermal treatment could activate a poor ZrO$_2$–WO$_3$ catalyst in the Friedel–Crafts reaction. Contrary trends were observed when using different solutions: the post-hydrothermal treatments with water or aqueous ammonium chloride reduced the acidity and activity, whereas, the treatments with ammonia solution or ethylenediamine solution largely improved the performance. The mechanism behind these changes was carefully addressed.

Experimental

Catalyst preparation

ZrO$_2$–WO$_3$ catalyst samples were synthesized by sol–gel process.[21] Firstly, 9 mmol Zr(OBu)$_4$ (TBOZ) and 1 mmol WCl$_6$ were dissolved in 30 mL ethanol containing 4.6 mL acetic acid and 2 mL hydrochloric acid at 25 °C. The sol was stirred for 2 h and evaporated at 30 °C to get the gel. After that, it was aged for 24 h at 65 °C to get the as-synthesized ZrO$_2$–WO$_3$ (A-ZrO$_2$–WO$_3$). Finally, the sample was calcined in air at 550 °C for 5 h. The resulting catalyst was denoted as ZrO$_2$–WO$_3$.

Post-synthesis treatment of ZrO$_2$–WO$_3$ by hydrothermal process (ZrO$_2$–WO$_3$-S, "S" indicates the solute, AH: ammonium

hydroxide, EDA: ethylenediamine, W: water, AC: ammonium chloride). The suspension of 3.0 g A-ZrO₂–WO₃ and 30 mL solution was transferred into a stainless Teflon-lined 100 mL capacity autoclave. The autoclave was subjected to hydrothermal treatment at 200 °C for 24 h. The products after the hydrothermal treatment was filtered and thoroughly washed with deionized water till the pH value of the filtered liquid was 7, and the powder was calcined in air at 550 °C for 5 h. The pH value for ammonium hydroxide, ethylenediamine, water and ammonium chloride aqueous solution is 12, 12, 7 and 5 respectively.

Characterization methods

X-ray diffraction (XRD) patterns were recorded on an Ultima IV diffractometer with Cu Kα radiation at 3 KW, a step size of 0.02°, scanning speed is 10° min⁻¹. Raman spectroscopy was obtained on HORIBA Scientific LabRAM HR Evolution with a visible (514.532 nm) laser excitation. The visible excitation was generated by an Ar excitation light source. The laser power was adjusted to 10 mW. Nitrogen adsorption–desorption analysis was carried out at 77 K on Nova 4200 e. All samples were

$$\text{Conversion of BA} = \frac{\text{Initial BA mole amount} - \text{Residual BA mole amount}}{\text{Initial BA mole amount}} = 1 - \frac{A_{i.Res}}{A_{i.Ini}}$$

pretreated at 300 °C under vacuum condition for 3 h and then they went through N₂ adsorption and desorption. X-ray

photoelectron spectroscopy (XPS) was carried out on a Thermo Scientific K-Alpha spectrometer equipped with Al Kα X-ray source (1486.6 eV). The base pressure during the analysis was 5×10^{-7} mBar. The C 1s line at 284.80 eV was used as an internal standard for the correction of binding energies (BE). Transmission electron microscopy analysis (HRTEM) of the samples was conducted on a JEOL 2010 transmission electron microscope operating at 200 kV. The samples were dispersed in high-purity ethanol and supported on carbon-coated copper grids for TEM. High angle annular dark field (HAADF) STEM was acquired with an aberration-corrected Titan ChemiSTEM equipped with a probe corrector (CEOS). This microscope was operated at 200 kV with an optimum attainable resolution of 0.078 nm.

The acid properties of the samples were determined by temperature-programmed desorption of ammonia (NH₃-TPD). NH₃-TPD was carried out on the Bel Cata II with a thermal conductivity detector. The 125 mg samples were pretreated at 573 K in dry air for 1 h and then cooled in flowing helium at 50 °C for 1 h. The ammonia adsorption was carried out for 1 h, using a NH₃/He (10% v/v) mixture gas. Weakly bound ammonia was removed by blowing-off with helium at a temperature of

50 °C for 1 h. NH₃-TPD was conducted in the temperature range of 50–550 °C with heating rate 10 °C min⁻¹.

Temperature-programmed reduction (TPR) was performed using an AutoChem1 II 2920 instrument (Thermo Fisher). The 0.050 g fresh sample was treated in a stream of He (50 mL min⁻¹), ramping the temperature at 10 °C min⁻¹ from room temperature to 300 °C and maintaining 300 °C for 1 h, and then cooled to 50 °C. The TPR measurement was carried out using H₂/Ar (10% v/v) as reducing gas mixture, flowing at 50 mL min⁻¹. The heating rate was 10 °C min⁻¹ from 50 °C to 800 °C.

Acid-catalyzed reaction

The Friedel–Crafts reaction of anisole and benzyl alcohol (BA for short) was carried out in a three-necked flask reactor at 122 °C. The reaction system was 0.1 g of catalyst, 50 mmol of anisole, and 5 mmol of BA. The concentration of each substrate was analyzed by a gas chromatograph (GC-2014, Shimadzu) equipped with a capillary column with n-decane as an internal standard. The BA conversion and selectivity were calculated by the following equation by internal standard method.[21]

where $A_{i.Res}$ is residual BA peak area, $A_{i.Ini}$ is initial BA peak area.

$$S\% = \frac{ortho - \text{benzylanisole} + para - \text{benzylanisole}}{ortho - \text{benzylanisole} + para - \text{benzylanisole} + \text{dibenzylether}} \times 100\%$$

Results and discussion

A ZrO₂–WO₃ sample was firstly prepared by a sol–gel method and then treated in a hydrothermal condition with an aqueous solution of ammonia (the obtained sample was named ZrO₂–WO₃-AH). The XRD patterns in Fig. 1a show that the prepared ZrO₂–WO₃ contains both tetragonal ZrO₂ (t-ZrO₂, patterns at 30.1° and 35.1°) and monoclinic ZrO₂ (m-ZrO₂, patterns at 28.2° and 31.4°), and the ratio of t-ZrO₂/m-ZrO₂ is 3.26. After the post-
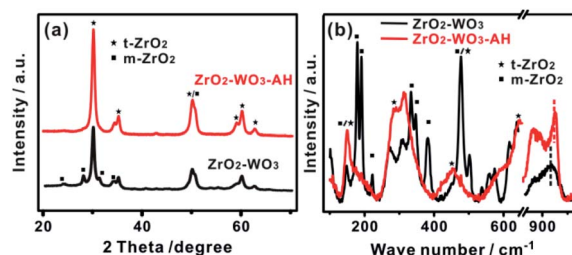

Fig. 1 (a) XRD patterns and (b) Raman spectra of ZrO₂–WO₃ and ZrO₂–WO₃-AH.

hydrothermal treatment, the intensity of m-ZrO$_2$ was almost diminished while that of t-ZrO$_2$ was enhanced, showing a final t-ZrO$_2$/m-ZrO$_2$ ratio of 6.85. No evident signal from tungsten-based materials (such as WO$_3$) could be observed despite that a considerable amount of W precursor (*i.e.*, atomic ratio W/Zr = 1/9) was added in the synthesis. This indicated a poor crystallinity or a high dispersion of W species in the product.

The catalysts were further characterized by Raman spectroscopy, which is more sensitive than XRD in characterizing the short-range order of nano-materials. As the results in Fig. 1b shown, t-ZrO$_2$ and *m*-ZrO$_2$ phases shared strong overlapping bands at 478 and 637–647 cm^{-1}, ZrO$_2$–WO$_3$ presented obvious m-ZrO$_2$ phase (characteristic peaks are at 179, 191, 220, 383 and 638 cm^{-1}), while ZrO$_2$–WO$_3$-AH contained the features of crystalline t-ZrO$_2$ phase with bands at 148, 285, 315 and 460 cm^{-1}, consistent with the XRD results.[22] Moreover, no crystalline WO$_3$ bands at 800, 708 and 265 cm^{-1} were observed in both samples, but only a broad band at 910–950 cm^{-1} that assigned to the W–O–Zr bond vibrations[23] and a peak at 950–1020 cm^{-1} that related to the stretching mode of terminal W=O bonds formed.[24] This confirmed the presence of W species that had a chemical interaction with ZrO$_2$. The Raman band shifts from 956 cm^{-1} in ZrO$_2$–WO$_3$ to 976 cm^{-1} in ZrO$_2$–WO$_3$-AH reflected the transformation of surface mono-tungstate to poly-tungstate species.[25–27] XRD and Raman results give valid evidence for the structural change of ZrO$_2$–WO$_3$ under hydrothermal treatment.

The morphology of both samples was characterized by electron microscopy. The representative HRTEM image of ZrO$_2$–WO$_3$ in Fig. 2a and ZrO$_2$–WO$_3$-AH in Fig. 2d show uniform lattice fringes: the lattice spacing of 0.294 and 0.303 nm were corresponded to the (110) planes of the t-ZrO$_2$, while the lattice spacing of 0.368 and 0.375 nm were corresponded to the (111) planes of m-ZrO$_2$. No tungsten oxide could be seen in this HRTEM mode. However, by changing to a STEM-HAADF mode, one can clearly see a spontaneous dispersion of bright spots on the surface of both samples (Fig. 2b and e).These spots with brighter contrast were proposed to be W species as W atoms are heavier than Zr atoms. It was important to note that the clear edge of the spots in ZrO$_2$–WO$_3$ became fuzzy after the hydrothermal treatment, possibly forming WO$_x$–Zr clusters at the

ZrO$_2$–WO$_3$ interface. The elemental mapping in Fig. 2c and f shows a homogenous dispersion of Zr on the sample, while the W signal was relatively stronger in the regions with bright spots. Consistent with the HAADF results, the W dispersed more evenly on ZrO$_2$ after the hydrothermal treatment. The XPS analysis of both samples indicated a 6+ state of W, suggesting that the W-rich clusters were dominated by WO$_3$.[26] (Fig. S1†).

The catalytic performance of the two catalysts were evaluated in the classic F–C reaction of anisole and benzyl alcohol (BA for short) to produce *ortho*-benzylanisole and *para*-benzylanisole, which are key industrial compounds as pharmaceutical intermediates or fine chemicals.[28] Basically, the activity of this reaction was determined by the strength or amount of Brønsted acid sites on the catalyst.[29] The catalytic results showed that *ortho*-benzylanisole, *para*-benzylanisole and dibenzylether (a byproduct) were all produced. The activity that calculated based on the conversion of BA after 0.5 h (Fig. 3a) indicated that ZrO$_2$–WO$_3$-AH (32.4%) was 8.76 times higher than that of the ZrO$_2$–WO$_3$ (3.7%). The activity of ZrO$_2$–WO$_3$-AH is comparable to the ZrO$_2$–WO$_3$ with hexadecyl trimethyl ammonium bromide as surfactant (39.2%) synthesized in our previous paper,[30] lower than sulfated zirconia.[31] But, ZrO$_2$–WO$_3$ is much more stable than the sulfated ones and less deactivate during catalytic reaction. Some other solid catalysts already known to catalyze Friedel–Crafts arylation reaction of anisole with benzyl alcohol are shown in Table S1.† ZrO$_2$–WO$_3$-AH exhibited lower price or higher activity. The five-cycle stability tests of ZrO$_2$–WO$_3$-AH sample in Fig. S2† showed almost no loss of both the activity and selectivity, indicating good stability and recyclability of the catalyst.

Considering the strong correlation between the activity and the Brønsted acid sites on the catalysts, we firstly tried to analyze the acidity of the catalysts before and after the hydrothermal treatment by using NH$_3$-TPD, for which, higher desorption temperature of NH$_3$ indicated stronger acidity. As the results shown in Fig. 3b, the NH$_3$ desorption profile could be roughly divided into two regions: <320 °C and >320 °C, which could be defined as "weak" and "strong" acid sites, respectively. The post-hydrothermal treatment with ammonia resulted in stronger desorption of NH$_3$ but with peaks at the same temperatures. This possibly indicated an increased amount of acid sites, rather than stronger acidity of each site. The concentration of weak and strong acid sites increased roughly by 40.6% and 34.0%, respectively, calculated based on the areas of the peaks.
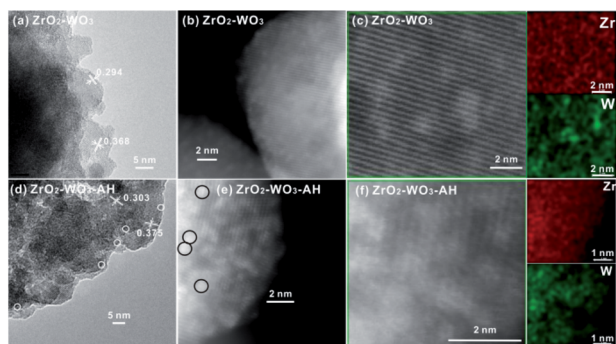

Fig. 2   (a and d) TEM, (b and e) HAADF and EDS (c and f) of ZrO$_2$–WO$_3$ and ZrO$_2$–WO$_3$-AH. White/black circles indicate WO$_x$ clusters with diameters of about 0.8 nm.

Fig. 3   (a) Friedel–Crafts reactions of anisole and benzyl alcohol and (b) NH$_3$-TPD of ZrO$_2$–WO$_3$ and ZrO$_2$–WO$_3$-AH.
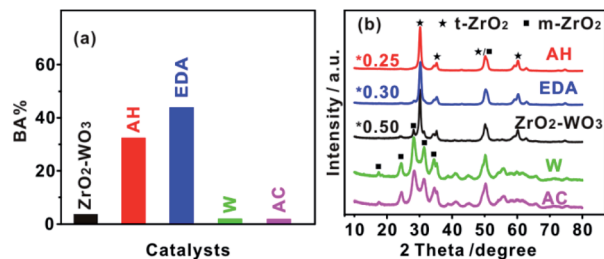
Paper

Fig. 4 (a) Friedel–Crafts reactions of anisole and benzyl alcohol (30 min), (b) XRD patterns for ZrO_2–WO_3 and ZrO_2–WO_3 post-treated with different solutions.

Fig. 5 Raman spectra of ZrO_2–WO_3 and ZrO_2–WO_3-S.

To find the correlation between the catalytic activity and the hydrothermal solutions used, the ZrO_2–WO_3 was post-treated with a series of other solutions, including pure water (sample named ZrO_2–WO_3-W), ammonium chloride (sample named ZrO_2–WO_3-AC), and ethylenediamine (sample named ZrO_2–WO_3-EDA). Strong base sodium hydroxide was not considered as hydrothermal medium because it would lead to the leaching of WO_3. The catalytic performance of these materials is displayed in Fig. 4a and Table 1. Basically, ZrO_2–WO_3-EDA and ZrO_2–WO_3-AH showed superior conversions of BA and similar selectivity to ZrO_2–WO_3, while both the conversion of BA and selectivity over ZrO_2–WO_3-W and ZrO_2–WO_3-AC were lower. The same trend was observed in yield of all catalysts as BA conversion. The yield values follow the order ZrO_2–WO_3-EDA > ZrO_2–WO_3-AH $\gg$ ZrO_2–WO_3 > ZrO_2–WO_3-W $\sim$ ZrO_2–WO_3-AC. Such a big impact of hydrothermal solutions in tailoring the catalytic performance of ZrO_2–WO_3 has never been reported to the best of our knowledge.

We firstly tried to understand the effects of surface area and valence state of W. The surface areas that calculated based on N_2 adsorption–desorption curves (Fig. S3a†) showed a significant increase after all the post-hydrothermal treatments no matter what solution was used (Table 1). However, ZrO_2–WO_3-W and ZrO_2–WO_3-AC with the largest surface areas performed the worst activity, claiming that the increase of surface area did not directly contribute to the reaction. In addition, the pore size was not likely proportional to the catalytic activity difference of all catalysts either (Fig. S3b†). On the other hand, the presence of ammonia species was reported to favour the formation of W^{5+} ions during annealing at high temperatures and these W^{5+} ions were responsible for the acidic properties as well as the activity
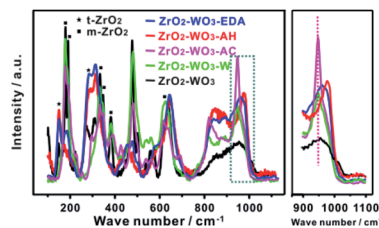
towards the F–C reaction. However, our XPS analysis on ZrO_2–WO_3 and ZrO_2–WO_3-AH clearly showed that only W^{6+} was present in both samples (Fig. S1†), also ruling out this possibility.

We then focused on the structural changes after post-hydrothermal treatments. The XRD patterns and Raman spectra of all the samples are displayed in Fig. 4b and 5. Both results showed that ZrO_2–WO_3-AH and ZrO_2–WO_3-EDA were dominated by t-ZrO_2, whereas ZrO_2–WO_3-W and ZrO_2–WO_3-AC contained almost only m-ZrO_2. This converse structures and their good correlation with the catalytic performance highly suggested that t-ZrO_2 was beneficial to the F–C reaction. Comparing to ZrO_2–WO_3, the frequency shift of the Raman bands from 956 to 967 cm^{-1} with the hydrothermal under EDA indicated that the W interaction species are polymeric (Fig. 5), similar to ZrO_2–WO_3-AH; whereas no obvious difference at this peak is detected in ZrO_2–WO_3-AC and ZrO_2–WO_3-W. To further verify the effect of hydrothermal solution on the crystal structure and the activity, we performed the same post-hydrothermal treatments on a ZrO_2–WO_3 that was calcined at 800 °C (sample named as ZrO_2–WO_3-800), a temperature that was high enough to caused crystalline WO_3 (XRD in Fig. S4†). As the results shown in Table S2 and Fig. S4,† the changes of the ZrO_2 structure and the catalytic activity were basically the same with ZrO_2–WO_3 when treating with the same solutions. It is interesting to note that the crystalline WO_3 in ZrO_2–WO_3-800 was retained after the post-hydrothermal treatments with water or NH_4Cl, yet it was not detected at all in ZrO_2–WO_3-EDA-800 and ZrO_2–WO_3-AH-800. This suggested a re-dispersion of WO_3 accompanied with the transformation of ZrO_2 crystalline phase in the EDA or ammonia solution.

We postulated that the formation of WO_x clusters and t-ZrO_2 was highly related to the pH value of the aqueous solution, as

Table 1 The structure–performance correlation of the BA conversion

Catalyst	BA%	S%	Y%[a]	$I_{t/m}$[b]	t-ZrO_2 size[c] (nm)	Surface area ($m^2\ g^{-1}$)
ZrO_2–WO_3	3.7	78.7	2.9	3.26	13.1	35.5
ZrO_2–WO_3-AH	32.4	77.7	25.2	6.85	12.2	54.0
ZrO_2–WO_3-EDA	43.9	78.2	34.3	5.88	10.9	65.2
ZrO_2–WO_3-W	1.97	62.7	1.2	$\sim$0	—	74.9
ZrO_2–WO_3-AC	1.86	64.6	1.2	$\sim$0	—	70.0

[a] Y% = conversion of BA × selectivity = BA% × S%. [b] Calculated by the equation $I_{t/m} = I_t/(I_{m1} + I_{m2})$ where I_t, I_{m1}, and I_{m2} represents the relative diffraction intensity of (101) plane of tetragonal zirconia, (111) plane and (111) plane of monoclinic zirconia. [c] Analyzed from XRD patterns.
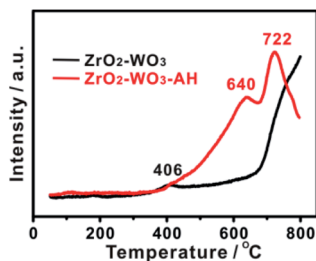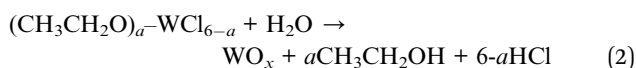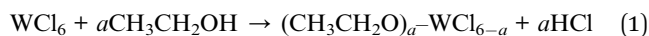
Fig. 6 H$_2$-TPR for ZrO$_2$–WO$_3$ and ZrO$_2$–WO$_3$-AH.

both the ammonia and EDA are alkaline solutions, whereas the water and NH$_4$Cl are neutral or acidic medium. Ethanediamine (EDA) can create hydroxyl ions due to thermal degradation during hydrothermal process. Ammonium hydroxide is a typical weak base and produces hydroxide ions. At high pH, the high concentration of hydroxide ion (OH$^-$) contributed to the formation of WO$_x$ clusters. WO$_x$ was thought to be synthesized through reactions (1) and (2).[32] These OH$^-$ ions reacted with formed HCl and generated water (H$_2$O) which induced the generation of WO$_x$. What's more, OH$^-$ ions would promote linking of WO$_x$ units, and led to more polymerized WO$_x$ clusters.[33] The effect of OH$^-$ was further confirmed by the particle size change of t-ZrO$_2$ crystals results from XRD analyses. In XRD patterns, the tetragonal ZrO$_2$ percentage increases and the crystallite size decreases with post-treated by ammonium hydroxide or ethylenediamine (Table 1). It is suggested WO$_x$ surface species inhibit ZrO$_2$ crystallite sintering, stabilize t-ZrO$_2$ crystallites and lead to smaller size of t-ZrO$_2$ than in pure ZrO$_2$–WO$_3$.[34,35]

$$WCl_6 + aCH_3CH_2OH \rightarrow (CH_3CH_2O)_a–WCl_{6-a} + aHCl \quad (1)$$

$$(CH_3CH_2O)_a–WCl_{6-a} + H_2O \rightarrow$$
$$WO_x + aCH_3CH_2OH + 6\text{-}aHCl \quad (2)$$

The formation of more WO$_x$ clusters induced by OH$^-$ ions can be verified by H$_2$-TPR. As observed, a peak centered on 406 °C in ZrO$_2$–WO$_3$ and ZrO$_2$–WO$_3$-AH could be attributed to first step of WO$_3$ reduction (Fig. 6). While, two peaks of ZrO$_2$–WO$_3$-AH sample, about 640 °C and 720 °C, ascribed to reduction of WO$_3$ species (amorphous and non-stoichiometric WO$_3$)[36,37] shift to lower reduction temperature, compared with the peak above 800 °C of ZrO$_2$–WO$_3$. The two reduction step suggested a growth of WO$_x$ with W–O–W linkages; because linked WO$_x$ are reduced at lower temperatures than isolated WO$_x$ species.[38] TPR results confirmed that larger and more interconnected WO$_x$ clusters of ZrO$_2$–WO$_3$-AH formed after ammonium hydroxide hydrothermal treatment.

Conclusions

In conclusion, post-hydrothermal treatments with different solutions were performed on a poor ZrO$_2$–WO$_3$ solid acid catalyst. It was found that the treatment with ammonium hydroxide or ethylenediamine significantly affected the structure and

acidity of ZrO$_2$–WO$_3$, resulting in higher activity in F–C reaction. The treatment with water or ammonium chloride, in opposite, led to deactivation. High pH values were proposed to play the essential role in the regulation of crystal structure and acidic sites, and improved the uniformity of WO$_x$ species and prevented the formation of m-ZrO$_2$ during calcination. Our work demonstrated that even a low activity of ZrO$_2$–WO$_3$ catalyst can be activated by performing a suitable hydrothermal treatment. The formation of these acidic sites controlled by adjusting a hydrothermal condition rationally is of great importance in the design of solid acid catalyst.

Author contributions

Sha Li designed the experiment, analysed the data, wrote the manuscript and provided the funding acquisition. Ruopeng Yu, Bonan Xu, Zhikun Wang, conducted the experiments. Chunzheng Wu, Jianzhong Guo designed the experiment and reviewed the manuscript.

Conflicts of interest

There are no conflicts of interest to declare.

Acknowledgements

References

1 M. Hino and K. Arata, *Chem. Lett.*, 1979, **8**, 477–480.
2 M. Hino and K. Arata, *J. Chem. Soc., Chem. Commun.*, 1988, **18**, 1259–1260.
3 M. Hino and K. Arata, *J. Chem. Soc., Chem. Commun.*, 1988, **17**, 1168–1169.
4 W. J. Ji, J. Q. Hu and Y. Chen, *Catal. Lett.*, 1998, **53**, 15–21.
5 N. Soultanidis, W. Zhou, A. C. Psarras, A. J. Gonzalez, E. F. Iliopoulou, C. J. Kiely, I. E. Wachs and M. S. Wong, *J. Am. Chem. Soc.*, 2010, **132**, 13462–13471.
6 J. G. Santiesteban, J. C. Vartuli, S. Han, R. D. Bastian and C. D. Chang, *J. Catal.*, 1997, **168**, 431–441.
7 R. Kourieh, S. Bennici, M. Marzo, A. Gervasini and A. Auroux, *Catal. Commun.*, 2012, **19**, 119–126.
8 E. I. Ross-Medgaarden, W. V. Knowles, T. Kim, M. S. Wong, W. Zhou, C. J. Kiely and I. E. Wachs, *J. Catal.*, 2008, **256**, 108–125.
9 R. Sakthivel, H. Prescott and E. Kemnitz, *J. Mol. Catal. A: Chem.*, 2004, **223**, 137–142.
10 T. Y. Kim, D. S. Park, Y. Choi, J. Baek, J. R. Park and J. Yi, *J. Mater. Chem.*, 2012, **22**, 10021–10028.
11 M. Scheithauer, R. K. Grasselli and H. Knozinger, *Langmuir*, 1998, **14**, 3019–3029.

12 M. A. Cortes-Jacome, C. Angeles-Chavez, E. Lopez-Salinas, J. Navarrete, P. Toribio and J. A. Toledo, *Appl. Catal., A*, 2007, **318**, 178–189.

13 W. D. Sun, Z. B. Zhao, C. Guo, X. K. Ye and Y. Wu, *Ind. Eng. Chem. Res.*, 2000, **39**, 3717–3725.

14 P. Afanasiev, C. Geantet, M. Breysse, G. Coudurier and J. C. Vedrine, *J. Chem. Soc., Faraday Trans.*, 1994, **90**, 193–202.

15 M. Hartmanova, I. Travenec, A. A. Urusovskaya, K. Putyera, D. Tunega and I. I. Korobkov, *Solid State Ionics*, 1995, **76**, 207–214.

16 G. K. Chuah, S. Jaenicke and B. K. Pong, *J. Catal.*, 1998, **175**, 80–92.

17 H. Armendariz, M. A. Cortes, I. Hernandez, J. Navarrete and A. Vazquez, *J. Mater. Chem.*, 2003, **13**, 143–149.

18 H. Wang, Y. Wu, L. He and Z. Liu, *Energy Fuels*, 2012, **26**, 6518–6527.

19 M. A. Cortes-Jacome, J. A. Toledo, C. Angeles-Chavez, M. Aguilar and J. A. Wang, *J. Phys. Chem. B*, 2005, **109**, 22730–22739.

20 Y. Song, C. Kang, Y. Feng, F. Liu, X. Zhou, R. Dong and L. Xu, *Chin. J. Catal.*, 2008, **29**, 1196–1198.

21 S. Li, H. Zhou, C. Jin, N. Feng, F. Liu, F. Deng, J. Wang, W. Huang, L. Xiao and J. Fan, *J. Phys. Chem. C*, 2014, **118**, 6283–6290.

22 M. J. Li, Z. H. Feng, G. Xiong, P. L. Ying, Q. Xin and C. Li, *J. Phys. Chem. B*, 2001, **105**, 8107–8111.

23 W. Zhou, E. I. Ross-Medgaarden, W. V. Knowles, M. S. Wong, I. E. Wachs and C. J. Kiely, *Nat. Chem.*, 2009, **1**, 722–728.

24 I. E. Wachs, *Catal. Today*, 1996, **27**, 437–455.

25 R. A. Boyse and E. I. Ko, *J. Catal.*, 1997, **171**, 191–207.

26 J. R. Sohn and M. Y. Park, *Langmuir*, 1998, **14**, 6140–6145.

27 K. Song, H. Zhang, Y. Zhang, Y. Tang and K. Tang, *J. Catal.*, 2013, **299**, 119–128.

28 B. Yuan, W. Zhao, F. Yu and C. Xie, *Catal. Commun.*, 2014, **57**, 89–93.

29 C. Tagusagawa, A. Takagaki, A. Iguchi, K. Takanabe, J. N. Kondo, K. Ebitani, S. Hayashi, T. Tatsumi and K. Domen, *Angew. Chem., Int. Ed.*, 2010, **49**, 1128–1132.

30 S. Li, C. Jin, N. Feng, F. Deng, L. Xiao and J. Fan, *Catal. Commun.*, 2019, **123**, 54–58.

31 Z. Miao, J. Zhou, J. Zhao, D. Liu, X. Bi, L. Chou and S. Zhuo, *Appl. Surf. Sci.*, 2017, **411**, 419–430.

32 Y. Wang, X. Wang, Y. Xu, T. Chen and J. Liu, *Small*, 2017, **13**, 1603689.

33 G. Y. Guo, Y. L. Chen and W. J. Ying, *Mater. Chem. Phys.*, 2004, **84**, 308–314.

34 F. Di Gregorio and V. Keller, *J. Catal.*, 2004, **225**, 45–55.

35 L. M. Hernández-Pichardo, A. J. Montoya, P. del Angel, A. Vargas and J. Navarrete, *Appl. Catal., A*, 2008, **345**, 233–240.

36 A. M. Garrido Pedrosa, M. J. B. Souza, S. H. Lima, D. M. A. Melo, A. G. Souza and A. S. Araújo, *J. Therm. Anal. Calorim.*, 2007, **87**, 703–707.

37 D. G. Barton, S. L. Soled, G. D. Meitzner, G. A. Fuentes and E. Iglesia, *J. Catal.*, 1999, **181**, 57–72.

38 A. Martinez, G. Prieto, M. A. Arribas, P. Concepcion and J. F. Sanchez-Royo, *J. Catal.*, 2007, **248**, 288–302.